Publ. Astron. Soc. Japan (2016) 68 (2), 24 (1–13)
doi: 10.1093/pasj/psw002
Advance Access Publication Date: 2016 February 6

Angular momentum of the N_2H^+ cores in the Orion A cloud

Ken'ichi Tatematsu,[1,2,*] Satoshi Ohashi,[3] Patricio Sanhueza,[1] Quang Nguyen Luong,[1†] Tomofumi Umemoto,[1,2] and Norikazu Mizuno[1,3]

[1]National Astronomical Observatory of Japan, 2-21-1 Osawa, Mitaka, Tokyo 181-8588, Japan
[2]Department of Astronomical Science, SOKENDAI (The Graduate University for Advanced Studies), 2-21-1 Osawa, Mitaka, Tokyo 181-8588, Japan
[3]Department of Astronomy, The University of Tokyo, 7-3-1 Hongo, Bunkyo-ku, Tokyo 113-0033, Japan

*E-mail: k.tatematsu@nao.ac.jp
†East Asian Core Observatories Association (EACOA) Fellow

Received 2015 September 4; Accepted 2016 January 4

Abstract

We have analyzed the angular momentum of the molecular cloud cores in the Orion A giant molecular cloud observed in the N_2H^+ $J = 1$–0 line with the Nobeyama 45 m radio telescope. We have measured the velocity gradient using position–velocity diagrams passing through core centers, and made sinusoidal fits against the position angle. Twenty-seven out of 34 N_2H^+ cores allowed us to measure the velocity gradient without serious confusion. The derived velocity gradient ranges from 0.5 to 7.8 km s^{-1} pc^{-1}. We marginally found that the specific angular momentum J/M (against the core radius R) of the Orion N_2H^+ cores tends to be systematically larger than that of molecular cloud cores in cold dark clouds obtained by Goodman et al., in the J/M–R relation. The ratio β of rotational to gravitational energy is derived to be $\beta = 10^{-2.3\pm0.7}$, and is similar to that obtained for cold dark cloud cores in a consistent definition. The large-scale rotation of the $\int$-shaped filament of the Orion A giant molecular cloud does not likely govern the core rotation at smaller scales.

Key words: ISM: clouds — ISM: individual objects (Orion Molecular Cloud) — ISM: kinematics and dynamics — ISM: molecules — stars: formation

1 Introduction

Angular momentum J plays an essential role in the formation of stars (including binaries) and planets (e.g., Bodenheimer 1995). For molecular clouds and their internal cores, it is found observationally that the specific angular momentum J/M (angular momentum per unit mass) increases with increasing radius R in the power-law relation of $J/M \propto R^{1.6}$ (Goldsmith & Arquilla 1985; Goodman et al. 1993). It is suggested that the J/M–R relation is related to the linewidth–size (Δv–R) relation, one of the empirical relations found by Larson (1981)—see Goodman et al. (1993), Bodenheimer (1995). Because $J/M = I\omega/M = pRv_{\rm rot}$, the J/M–R relation can be expressed as $v_{\rm rot} \propto R^{0.6}$, which is very similar to the power-law form of the linewidth–size relation. Here, I is the moment of inertia, $v_{\rm rot}$ is the rotation velocity, ω is the angular velocity, and the parameter p is equal to $\frac{2}{5}$ for a uniform density sphere. When we use the observed linewidth Δv rather than non-thermal or total linewidth (see Fuller & Myers 1992 for the definition), the linewidth–size relation is expressed as $\Delta v = AR^a$ with $a \sim 0.4$–0.5, (e.g., Larson 1981; Fuller & Myers 1992; Blitz 1993). Here, A is a constant

or coefficient for the power-law relation (corresponding to the intercept in the log–log form, log Δv–log R relationship). The origin of the linewidth–size relation is still under debate, and many theoretical studies have been carried out. For example, Inoue and Inutsuka (2012) studied the formation of molecular clouds due to accretion of H I clouds through magnetohydrodynamic simulations including the effects of radiative cooling/heating, chemical reactions, and thermal conduction, and successfully reproduced the observed linewidth–size relation. Molecular clouds and their cores are thought to be near virial equilibrium (e.g., Larson 1981; Myers 1983). The ratio β of rotational to gravitational energies is found to be of the order of 0.02 for dark cloud cores (Goodman et al. 1993). Goodman et al. (1993) suggested that the J/M–R relation can be explained for virial equilibrium cores if β is constant against the core size. β and the ratio α of the thermal to gravitational energies is thought to affect the core fragmentation process, which will be related to the frequency of binary and multiple star formation (e.g., Miyama et al. 1984; Tsuribe & Inutsuka 1999; see also Matsumoto & Hanawa 2003).

Galactic molecular clouds can be divided into two categories: giant molecular clouds (GMCs) and cold dark clouds (excluding infrared dark clouds here; e.g., Shu et al. 1987; Turner 1988; Bergin & Tafalla 2007). These two categories of clouds show different ranges of cloud mass, and star-formation modes: GMCs are most likely associated with cluster star formation including massive stars, while cold dark clouds preferentially show isolated low-mass star formation. Furthermore, molecular cloud cores inside these clouds show different characteristics: warm-temperature, turbulent cores in GMCs, and cold thermal cores in cold dark clouds. It was suggested that the coefficient A (or intercept in the log–log form) of the linewidth–size relation differs between cores in these two categories. Tatematsu et al. (1993) have studied molecular cloud cores in the Orion A GMC in CS $J = 1$–0, and suggested that this coefficient A (or intercept) is larger in Orion cores compared with that for cores in cold dark clouds. They argued that a larger coefficient means that Orion cores have higher external pressure and/or stronger magnetic fields. Caselli and Myers (1995) have also suggested different intercepts (and different slopes) between GMC cores and cold dark cloud cores using the Orion A GMC data of Tatematsu et al. (1993) and other complementary data. Originally, Larson (1981) pointed out that the linewidth is relatively small in the Taurus cold dark cloud, larger in the ρ Ophiuchi complex, and even larger in the Orion A GMC (meaning different intercepts). Tatematsu (1999) compared the linewidth–size relation between "well-defined" Orion A GMC cores and cold dark cloud cores (see their figure 7) and concluded that the intercept is clearly different, but the power-law index is not so different. Further evidence of variation of intercept was obtained toward the Galactic Center, where the intercept is even larger than that for Orion cores (Tsuboi & Miyazaki 2012). Heyer et al. (2009), Ballesteros-Paredes et al. (2011), and Traficante et al. (2016) have also shown that the coefficient (or intercept) of the linewidth–size relation is highly related to the surface density (higher external pressure and/or stronger magnetic fields lead to higher surface density), and it has deviations among clouds. It seems that different coefficients (or intercepts) of the linewidth–size relation in different categories of Galactic clouds are well established.

Given that the intercept of the linewidth–size relation differs among Galactic clouds, we wonder whether the J/M–R relation also shows any difference. Tatematsu (1999) compared the J/M–R relation of the Orion CS cores with that for cold dark cloud cores derived in NH_3 by Goodman et al. (1993), and found that the Orion cores may have slightly larger J/M. However, their results were not conclusive because of large data scattering and insufficient linear-scale resolution in pc. In this paper, we re-investigate the difference in the J/M–R relation by using data obtained in N_2H^+ at higher angular resolution toward the Orion A GMC (Tatematsu et al. 2008). N_2H^+ and NH_3 are thought to trace similar volumes of dense gas (subsection 3.5).

In this work we adopt a distance of 418 ± 6 pc for the Orion A GMC, based on the work of Kim et al. (2008), as the best estimate rather than 450 pc as used in Tatematsu et al. (2008). At this distance, $1'$ corresponds to 0.122 pc. We correct the core radius (in pc) and core mass of Tatematsu et al. (2008) by decreasing them by 6.5% and 12.5%, respectively.

Table 1 lists the N_2H^+ cores in the Orion A GMC from Tatematsu et al. (2008). The kinetic temperature T_k is calculated from the rotation temperature from NH_3 observations of Wilson et al. (1999) and by using the conversion given in Danby et al. (1988). In general, N_2H^+ core positions do not match NH_3 observed positions, so we take the value of the nearest NH_3 position. The total linewidth Δv_{TOT}, including both thermal and non-thermal contribution, is calculated by using T_k and by correcting for the difference of the mean molecular mass (2.33 u) and the mass of the observed molecule (N_2H^+, 29 u; Fuller & Myers 1992). The core mass M is taken from Tatematsu et al. (2008), which was obtained by assuming local thermodynamic equilibrium (LTE) and corrected for the distance revision. The virial mass M_{vir} ($M_\odot$) is defined as 210 R (pc) Δv_{TOT}^2 (km s^{-1}) for a uniform density sphere (MacLaren et al. 1988). The virial parameter α_{vir} is defined as the ratio of the virial mass M_{vir} to the core mass M, and its average for Orion N_2H^+ cores is 0.79 ± 0.61 ($\log \alpha_{vir} = -0.21 \pm 0.31$).

Table 1. N_2H^+ cores in the Orion A GMC.

No.	RA (J2000.0)			Dec (J2000.0)			T_k	V_{LSR}	Δv	Δv_{TOT}	R	M	M_{vir}	α_{vir}
	(h	m	s)	(°	′	″)	(K)	(km s^{-1})	(km s^{-1})	(km s^{-1})	(pc)	($M_\odot$)	($M_\odot$)	
1	5	35	06.2	−4	54	24	–	11.1	0.65 ± 0.05	–	0.049	–	–	–
2	5	35	06.1	−4	56	07	–	11.2	0.62 ± 0.03	–	0.088	22	–	–
3	5	35	29.4	−4	58	31	30	12.3	1.31 ± 0.10	1.50	0.083	39	39	1.02
4	5	35	19.8	−5	00	53	16	11.3	0.57 ± 0.01	0.79	0.084	43	11	0.25
5	5	35	26.8	−5	01	13	22	11.5	0.79 ± 0.05	1.01	0.059	10	13	1.33
6	5	35	25.4	−5	02	36	24	11.1	0.51 ± 0.02	0.83	0.099	47	15	0.31
7	5	35	26.7	−5	05	00	28	11.6	0.47 ± 0.01	0.85	0.091	41	14	0.33
8	5	35	32.3	−5	06	02	34	11.8	0.74 ± 0.04	1.07	0.049	–	12	–
9	5	35	23.9	−5	07	25	26	11.9	0.86 ± 0.04	1.10	0.098	47	25	0.53
10	5	35	26.7	−5	10	09	28	11.3	1.23 ± 0.02	1.42	0.095	57	40	0.7
11	5	35	22.6	−5	10	09	–	11.7	0.62 ± 0.02	–	0.052	9	–	–
12	5	35	22.7	−5	12	32	28	11.0	0.93 ± 0.02	1.17	0.104	77	30	0.38
13	5	35	21.2	−5	14	36	19	10.8	0.62 ± 0.02	0.86	0.094	39	14	0.37
14	5	35	08.8	−5	18	41	24	9.0	0.62 ± 0.03	0.91	0.083	21	14	0.68
15	5	35	15.8	−5	19	26	30	9.9	1.31 ± 0.02	1.50	0.111	117	53	0.45
16	5	35	08.9	−5	20	22	–	8.6	2.05 ± 0.09	–	0.105	–	–	–
17	5	35	10.3	−5	21	25	–	8.1	1.08 ± 0.05	–	0.074	–	–	–
18	5	35	06.1	−5	22	46	–	7.4	2.06 ± 0.14	–	0.057	–	–	–
19	5	35	12.9	−5	24	10	61	6.6	2.12 ± 0.07	2.37	0.072	–	85	–
20	5	35	04.7	−5	24	13	26	8.6	1.92 ± 0.10	2.03	0.043	–	38	–
21	5	35	15.7	−5	25	54	55	8.2	1.15 ± 0.06	1.52	0.062	13	30	2.4
22	5	35	14.3	−5	26	56	40	8.8	1.72 ± 0.07	1.92	0.074	–	57	–
23	5	35	02.0	−5	36	10	24	7.3	0.32 ± 0.01	0.74	0.115	59	13	0.22
24	5	35	04.8	−5	37	32	16	8.8	0.72 ± 0.03	0.90	0.083	41	14	0.34
25	5	34	56.6	−5	41	39	–	3.7	0.48 ± 0.03	–	0.084	–	–	–
26	5	34	57.7	−5	43	41	24	7.1	0.41 ± 0.03	0.78	0.062	–	8	–
27	5	34	56.3	−5	46	05	24	5.5	1.11 ± 0.08	1.29	0.074	20	26	1.27
28	5	35	08.8	−5	51	57	16	7.0	0.38 ± 0.05	0.66	0.081	–	8	–
29	5	35	00.7	−5	55	40	–	8.0	0.49 ± 0.05	–	0.062	–	–	–
30	5	35	09.0	−5	55	41	34	7.5	0.64 ± 0.04	1.01	0.052	6	11	1.77
31	5	35	12.8	−5	58	06	16	7.6	0.83 ± 0.09	0.99	0.083	–	17	–
32	5	35	28.1	−6	00	09	–	7.3	0.35 ± 0.04	–	0.157	67	–	–
33	5	36	12.4	−6	10	44	34	8.2	0.62 ± 0.06	1.00	0.057	11	12	1.05
34	5	36	24.7	−6	14	11	21	8.2	0.92 ± 0.16	–	0.072	–	–	–

These do not deviate far from virial equilibrium. A blank (—) in the T_k column means that we do not have a good nearest NH_3 counterpart. A blank in the M column (and then Δv_{TOT}, M_{vir}, and α_{vir} columns) means either no T_k value or failure in the N_2H^+ hyperfine fit to restrict the optical depth.

2 Data and method

We use the data of N_2H^+ $J = 1$–0 cores (Tatematsu et al. 2008) obtained with the 45 m radio telescope of the Nobeyama Radio Observatory (NRO).[1] The half-power beam width of the telescope was 17.″8 ± 0.″4, and the spacing grid employed in mapping observations was 20.″55. The spectral resolution was 37.8 kHz (∼0.12 km s^{-1}). The core radius R is $\gtrsim$25″ or 0.05 pc, which is thought to imply the detection limit in the observations. Details of the observations and examples of N_2H^+ spectra can be found in Tatematsu et al. (2008). It is known that N_2H^+ traces the quiescent gas, and is less affected by depletion (Bergin et al. 2001, 2002) or by star-formation activities such as molecular outflows (e.g., Womack et al. 1993). Therefore, this molecular line is one of the best molecular lines to use for this study. On the other hand, in warm gas (temperature > 25 K), N_2H^+ will be destroyed by evaporated CO (Lee et al. 2004; Tatematsu et al. 2014).

Cores in the Orion A GMC are much more crowded compared with cores in dark clouds. If we use the core

[1] Nobeyama Radio Observatory is a branch of the National Astronomical Observatory of Japan, National Institutes of Natural Sciences.

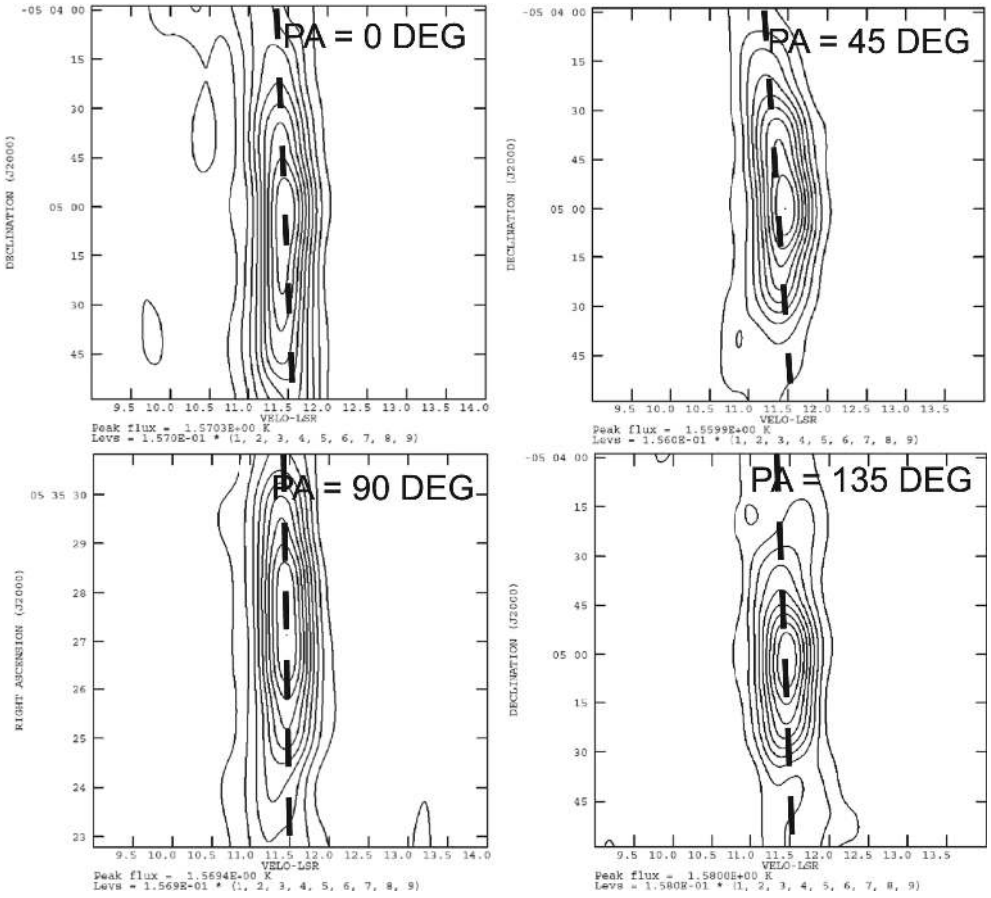

Fig. 1. Position–velocity diagram for N_2H^+ core 7. The abscissa is the LSR velocity (km s^{-1}) corresponding to N_2H^+ $J = 1$–0, F_1, $F = 0$, 1–1, 2. The thick dashed line shows the velocity gradient measured through visual inspection.

number surface density of $H^{13}CO^+$ cores (Ikeda et al. 2007; Onishi et al. 2002), the Orion A GMC and the Taurus molecular cloud, which are examples of crowded cold dark clouds, have 5 and 0.2 $H^{13}CO^+$ cores per pc^2, respectively, with a difference of the order of 25. Therefore, core identification and measurement of the velocity gradient are more difficult in the Orion A GMC.

We measured the velocity gradient as follows.

(a) We draw four position–velocity (PV) diagrams (position angles $PA = 0°$, $45°$, $90°$, and $135°$) passing through the core center.[2] We use the isolated hyperfine component N_2H^+ $J = 1$–0, F_1, $F = 0$, 1–1, 2, which is the line less affected by neighboring satellites (Caselli et al. 1995), to avoid confusion. Because the data was taken only on a regular grid (rather than on-the-fly mapping observations), the number of actually observed positions along the strip line depends on PA. Interpolation would introduce method-dependent uncertainties that we want to avoid. The interval of actually observed positions is $20''$ for PV diagrams at $PA = 0°$ and $90°$, and $28''.28$ ($= 20\sqrt{2}''$) at $PA = 45°$ and $135°$. The average half width at half maximum (HWHM) radius of N_2H^+ cores in Orion A GMC by Tatematsu et al. (2008) is $39''$. If we draw PV diagrams at $PA = 26°.57$ [$= \arctan(0.5)$], $63°.43$, $116°.57$, and $153°.44$, the interval of actually observed positions is $44''.72$ ($= 20\sqrt{5}''$), which is larger than the average core radius. Then, only PV diagrams at $PA = 0°$, $45°$, $90°$, and $135°$ contain a sufficient number of observed positions along strips. In summary, we prefer to use the strip line passing through actually observed grid positions, to reduce uncertainties caused by interpolation. Figures 1 and 2 show examples of PV diagrams.

(b) Next, we measure the velocity gradient mainly using the half-intensity (50%) peak contour through careful visual inspection, assuming rigid body rotation.

(b1) We check whether the half-intensity peak contour is confused by another core or not. If it is not confused, we determine the velocity gradient line by using the minimum and maximum velocities of the half-intensity peak contour.

[2] PV diagrams will be available through the website ⟨http://alma.mtk.nao.ac.jp/~kt/kt-e.html⟩.

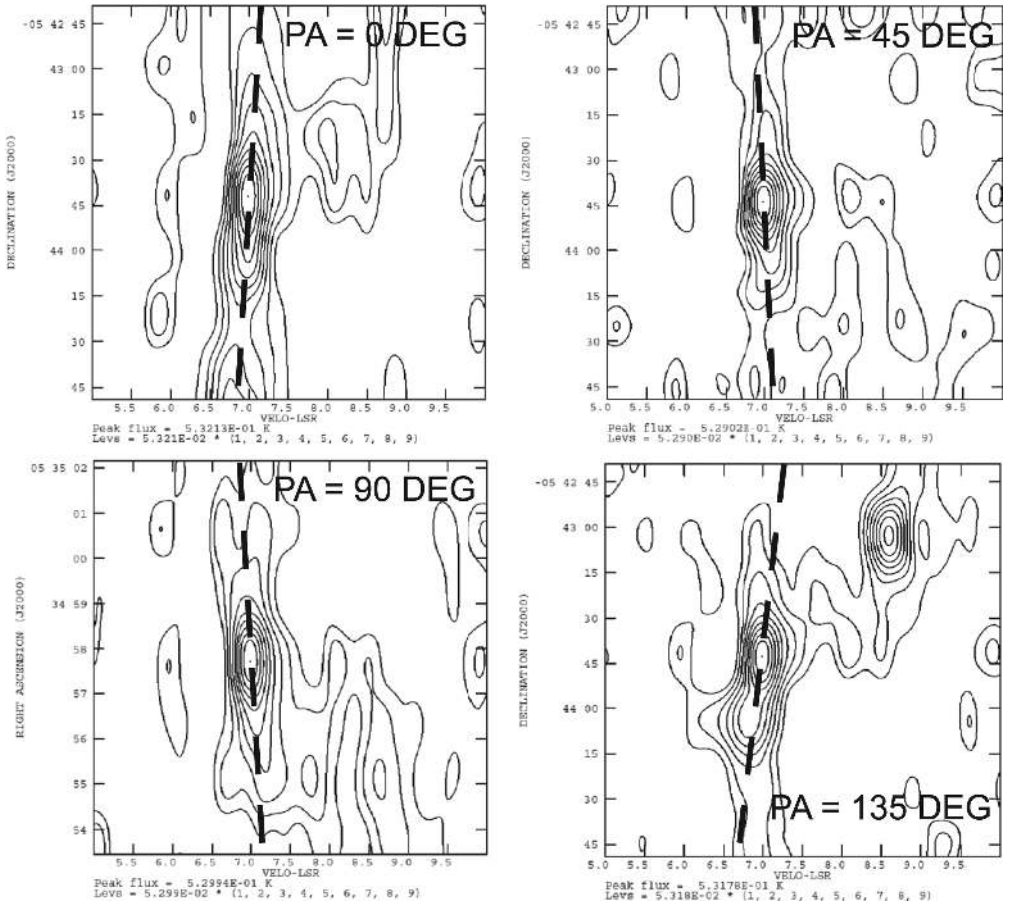

Fig. 2. Same as figure 1 but for N_2H^+ core 26.

(b2) If the half-intensity peak contour is symmetrical with respect to the velocity gradient line, we adopt it.

(b3) If the half-intensity contour is not smooth (i.e., irregular, distorted, or wavy in shape) near the minimum or maximum velocity point, we try to determine the velocity gradient line so that the half-intensity contour looks symmetrical to the line.

(b4) We also check the 60%, 70%, and 80% intensity peak contours. If their minimum and maximum velocities are fitted by another velocity gradient line, and if the 60%, 70%, and 80% contours are more symmetrical with respect to this velocity gradient line, we adopt it. The velocity gradient line does not necessarily pass through the core center, but we allow this if the candidate contour looks like an oval rather than a dogleg or very irregular shape as a whole.

We have measured the velocity gradient in 27 cores (out of 34 cores) without serious confusion with other cores/emission features spatially and in velocity.

(c) We fit a sinusoidal curve to the diagram of velocity gradient against *PA* through a non-linear least-squares fit. The amplitude of the sinusoidal function provides the intensity of the velocity gradient, while the angle at which the maximum is found describes the position angle of the velocity gradient. Figures 3 and 4 show examples of the sinusoidal fitting. The velocity gradient on the position–velocity diagram for each *PA* (0°, 45°,

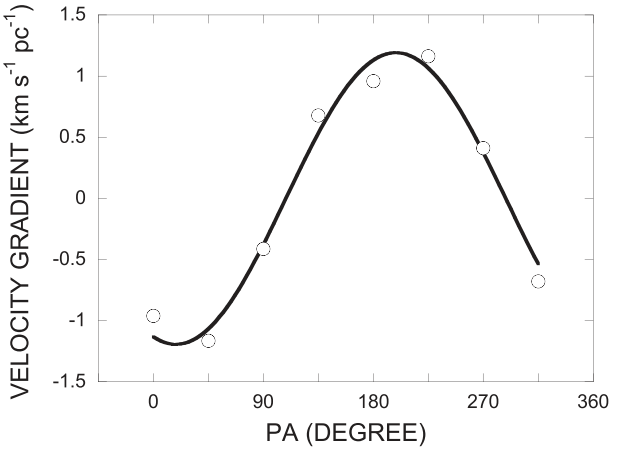

Fig. 3. Sinusoidal fit to the velocity gradient fit against *PA* for N_2H^+ core 7.

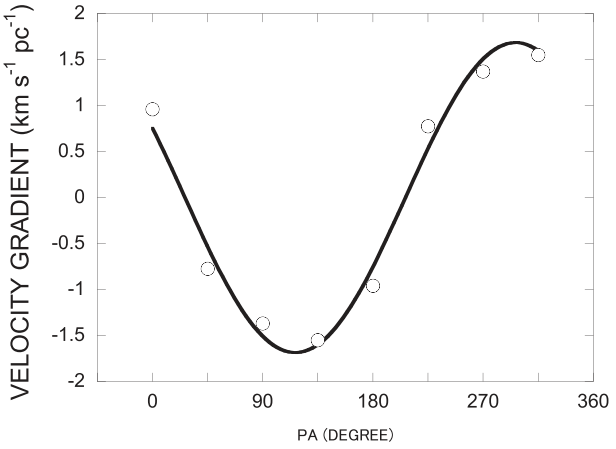

Fig. 4. Sinusoidal fit to the velocity gradient fit against *PA* for N_2H^+ core 26.

90°, and 135°) is plotted twice at *PA* and *PA* + 180° with opposite signs for the gradients.

Table 2 lists the result of the measurements. The N_2H^+ core number is taken from Tatematsu et al. (2008). A velocity gradient of "0" means that we cannot measure the gradient at each PV diagram because it is too small. β is the ratio of rotational to gravitational energies (see subsection 3.2). A blank (—) in the V Grad columns means that the velocity gradient is not measurable without confusion. A blank in the β column in table 2 means that the core mass was not accurately estimated in Tatematsu et al. (2008). The average physical parameters of velocity–gradient measurable cores are $T_{\rm ex} = 9.5 \pm 4.3$ K, $\Delta v = 0.82 \pm 0.44\,{\rm km\,s^{-1}}$, $R = 0.082 \pm 0.026$ pc, and $M = 42 \pm 28\,M_\odot$. The velocity gradient derived for 27 cores ranges from 0.5 to $7.8\,{\rm km\,s^{-1}\,pc^{-1}}$, and its average is $2.4 \pm 1.6\,{\rm km\,s^{-1}\,pc^{-1}}$.

3 Results and discussion

3.1 Specific angular momentum against radius

We define the specific angular momentum as $J/M = I\omega/M = \frac{2}{5}Rv_{\rm rot}$ for a uniform density sphere. Because the moment of inertia I is proportional to mass M, J/M can be derived without using the mass estimate. In figure 5, we plot the specific angular momentum against core radius. The core radius R of Orion cores is measured as $R = \sqrt{S/\pi}$, where S is the area within the half-intensity contour, and then corrected for the telescope beam size (Tatematsu et al. 2008). The data for cold dark cloud cores are taken from Goodman et al. (1993). To do an appropriate comparison, we need to use common definitions for physical parameters. We therefore convert the geometrical mean of the two-dimensional FWHM diameter in Goodman et al. (1993) to the HWHM radius (FWHM/2) R in our study. Goodman et al. (1993) also corrected the radius for the telescope beam size (deconvolved size). If the velocity gradient $v_{\rm rot}/R$ is constant against R, J/M increases as R^2 from the definition. Therefore, we divide J/M as listed in Goodman et al. (1993) by a factor of four for consistency. The ratio β of rotational to gravitational energies is calculated consistently. Table 2 lists the results.

Figure 5 shows that Orion cores are mostly located above the least-squares fit of cold dark cloud cores. The results of linear least-squares fitting are:

$$\log J/M\,({\rm cm^2\,s^{-1}}) = 21.31 \pm 0.07 + 1.24 \pm 0.38 \log(R/0.1\ {\rm pc}) \quad (1)$$

for Orion cores,

$$\log J/M\,({\rm cm^2\,s^{-1}}) = 21.15 \pm 0.05 + 1.65 \pm 0.20 \log(R/0.1\ {\rm pc}) \quad (2)$$

for cold dark cloud cores. The number of Orion N_2H^+ cores located below the least-squares fit for cold dark cloud cores is relatively small. Tatematsu (1999) showed very similar results for Orion cores using the CS $J = 1$–0 mapping data of Tatematsu et al. (1993). The power-law index is less certain in Orion cores compared with cold dark cloud cores, because of a narrower core radius range. If we assume a power-law index of 1.65 obtained for cold dark cloud cores also for Orion cores, we obtain

$$\log J/M\,({\rm cm^2\,s^{-1}}) = 21.35 \pm 0.05 + 1.65 \log(R/0.1\ {\rm pc}) \quad (3)$$

for Orion cores (see figure 6). To confirm the results of these fits, we now only use cores with $R \geq 0.05$ pc and $v_{\rm rot} \geq 0.08\,{\rm km\,s^{-1}}$, which are the approximate detection limits in the velocity gradient measurement in Orion, for both Orion cores and cold dark cloud cores. The beam-deconvolved radius $R = 0.05$ pc corresponds to 24″.6, which is 1.4 times the telescope beamsize, and 1.2 times the grid spacing of the observations. We measure the velocity gradient by using the minimum and maximum velocities on both sides with respect to the core center. The difference between the minimum and maximum velocities is 2 $v_{\rm rot}$, which corresponds to a length of twice the half-intensity peak radius. We can measure the velocity difference 2 $v_{\rm rot}$ at the half-intensity peak down to 2.5–3 times the instrumental resolution ($\sim 0.12\,{\rm km\,s^{-1}}$), and the detection limit is approximately $v_{\rm rot} = 0.08\,{\rm km\,s^{-1}}$. Figure 7 shows the J/M–R relation. The results of linear least-squares fitting

Table 2. Velocity gradient and angular momentum of the Orion A GMC N_2H^+ cores.

No.	V Grad				V Grad *PA* (fit)	V Grad (fit)	v_{rot}	J/M	β
	$PA = 0°$ (km s^{-1} pc^{-1})	$PA = 45°$ (km s^{-1} pc^{-1})	$PA = 90°$ (km s^{-1} pc^{-1})	$PA = 135°$ (km s^{-1} pc^{-1})	(°)	(km s^{-1} pc^{-1})	(km s^{-1})	(cm^2 s^{-1})	
1	0	1.26	2.19	2.52	100.5 ± 4.8	2.5 ± 0.2	0.12 ± 0.01	7.4E+20	–
2	− 0.69	0	0	3.05	143.8 ± 17.1	1.8 ± 0.5	0.16 ± 0.05	1.7E+21	7.6E−03
3	− 0.96	1.26	1.1	− 0.19	87.9 ± 25.5	0.9 ± 0.4	0.07 ± 0.03	7.6E+20	9.3E−04
4	0	− 0.78	− 1.1	0.44	237.3 ± 17.9	0.8 ± 0.2	0.07 ± 0.02	7.2E+20	7.3E−04
5	–	–	–	–	–	–	–	–	–
6	0.27	0	− 0.96	0	286 ± 23.4	0.5 ± 0.2	0.05 ± 0.02	6.0E+20	4.0E−04
7	− 0.96	− 1.16	− 0.41	0.68	198.4 ± 3.4	1.2 ± 0.1	0.10 ± 0.01	1.2E+21	1.9E−03
8	6.44	0	− 2.06	− 3.88	332.4 ± 8.5	5.2 ± 0.7	0.26 ± 0.04	1.6E+21	–
9	− 5.07	− 7.85	− 5.89	0.68	224.6 ± 1.9	7.8 ± 0.2	0.77 ± 0.02	9.3E+21	9.5E−02
10	1.64	1.74	− 1.64	− 3.2	332.5 ± 7.8	2.9 ± 0.4	0.27 ± 0.04	3.2E+21	9.7E−03
11	1.23	0.63	0	0	14.9 ± 12.2	0.9 ± 0.2	0.05 ± 0.01	3.0E+20	9.7E−04
12	2.33	0	− 1.78	− 0.53	321.4 ± 16.3	1.7 ± 0.5	0.18 ± 0.05	2.3E+21	3.3E−03
13	− 0.69	− 0.78	− 2.47	0	247.8 ± 13.8	1.6 ± 0.4	0.15 ± 0.04	1.8E+21	4.5E−03
14	1.92	2.81	0	− 1.55	10.1 ± 6.8	2.5 ± 0.3	0.21 ± 0.03	2.2E+21	1.3E−02
15	− 0.96	− 0.29	− 1.78	− 1.02	260.7 ± 14.5	1.4 ± 0.3	0.16 ± 0.04	2.1E+21	1.8E−03
16	0.96	− 3.97	0	1.16	216.7 ± 14.5	1.4 ± 0.3	0.15 ± 0.03	1.9E+21	–
17	2.33	0	0	− 4.75	329.4 ± 12.4	3.3 ± 0.7	0.24 ± 0.05	2.2E+21	–
18	–	–	–	–	–	–	–	–	–
19	–	–	–	–	–	–	–	–	–
20	1.03	− 7.37	0	3.39	203.1 ± 29.7	3.6 ± 1.9	0.16 ± 0.08	8.4E+20	–
21	0	− 6.4	0	− 1.74	240.3 ± 23.4	3.3 ± 1.3	0.20 ± 0.08	1.5E+21	1.6E−02
22	–	–	–	–	–	–	–	–	–
23	1.1	1.45	0	0	25.8 ± 10.2	1.2 ± 0.2	0.13 ± 0.03	1.9E+21	2.6E−03
24	− 4.93	− 2.23	0.27	5.14	167.1 ± 4.1	5.2 ± 0.3	0.43 ± 0.03	4.4E+21	2.9E−02
25	–	–	–	–	–	–	–	–	–
26	0.96	− 0.78	− 1.37	− 1.55	296.6 ± 3.4	1.6 ± 0.1	0.10 ± 0.01	7.7E+20	–
27	–	–	–	–	–	–	–	–	–
28	− 0.69	0	0.62	1.94	136 ± 8.3	1.4 ± 0.2	0.11 ± 0.02	1.1E+21	–
29	2.47	1.65	2.47	0	45 ± 8.4	2.5 ± 0.4	0.16 ± 0.03	1.2E+21	–
30	0.96	4.46	1.58	1.45	61.8 ± 10.2	3.3 ± 0.6	0.17 ± 0.03	1.1E+21	1.9E−02
31	− 0.82	− 3.78	− 2.88	− 1.55	250.2 ± 3.9	3.5 ± 0.2	0.29 ± 0.02	3.0E+21	–
32	− 0.96	0	0	1.45	152.7 ± 10.8	1.2 ± 0.2	0.18 ± 0.04	3.5E+21	6.0E−03
33	− 0.96	0	− 3.7	− 1.07	267.4 ± 17.9	2.2 ± 0.7	0.13 ± 0.04	8.9E+20	6.3E−03
34	–	–	–	–	–	–	–	–	–

are:

$$\log J/M\,(\mathrm{cm^2\ s^{-1}}) = 21.38 \pm 0.06 + 1.23 \pm 0.42 \log(R/0.1\ \mathrm{pc}) \quad (4)$$

for Orion cores,

$$\log J/M\,(\mathrm{cm^2\ s^{-1}}) = 21.24 \pm 0.05 + 1.30 \pm 0.23 \log(R/0.1\ \mathrm{pc}) \quad (5)$$

for cold dark cloud cores. It seems that Orion cores have systematically larger J/M than cold dark cloud cores, although the difference is marginal. This trend is similar to what we see in the linewidth–size relation (Tatematsu et al. 1993). Our result may imply that non-thermal motions (turbulence) are related to the origin of angular momentum. Orion cores and cold dark cloud cores have a similar slope (1.2–1.3) in figure 7, but their values are shallower than the value of 1.6 found by Goodman et al. (1993) and Goldsmith and Arquilla (1985). This could be the result of a narrow core radius range after the restriction. In general, least-squares fitting tends to provide a shallower slope, if data scattering is large. Consider a case where x and y are positively correlated. We fit x–y data to a formula $y = ax + b$, and then fit again the data with the expression $x = cy + d$. We will obtain $c \sim 1/a$ if x and y are well correlated (the correlation coefficient is close to unity). If the data is very scattered

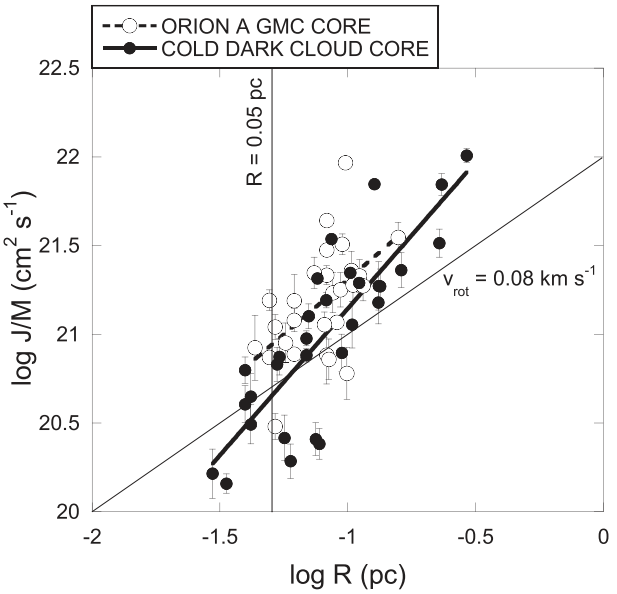

Fig. 5. J/M–R diagram for 27 Orion cores (open circles) and cold dark cloud cores (filled circles). The error bar represents uncertainties in measurements of the velocity gradient. The dashed and solid straight lines are computed using a linear least-squares program for Orion cores and cold dark cloud cores, respectively. Thin straight lines delineate approximate detection limits for Orion cores: $R = 0.05$ pc and $v_{\rm rot} = 0.08$ km s^{-1}.

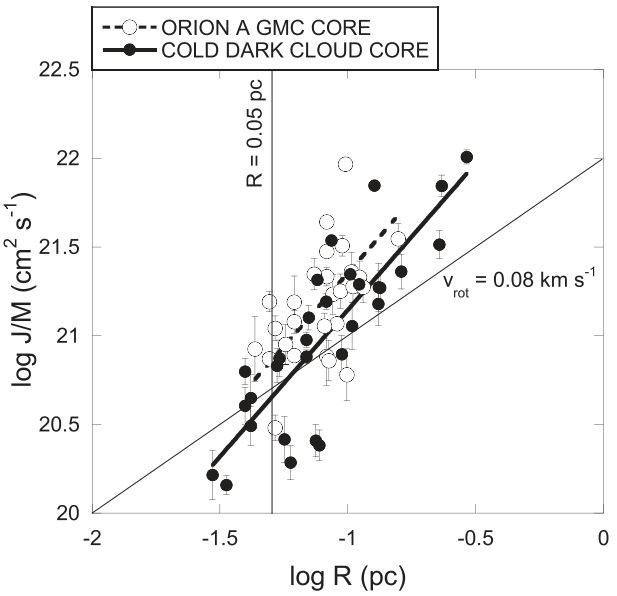

Fig. 6. Same as figure 5 but the best-fit line for Orion cores is obtained by fixing a slope (power-law index) of 1.65 obtained for cold dark cloud cores.

(the correlation coefficient is small), a will be smaller than $1/c$. This is because least-squares fitting minimizes the "vertical distances" between the observed points and the fitted points. By narrowing the range of the core radius R, scattering becomes larger. This explains why Orion cores show a shallower slope in figure 5, and why the slope of cold dark cloud cores becomes smaller in figure 7. If we fix the slope

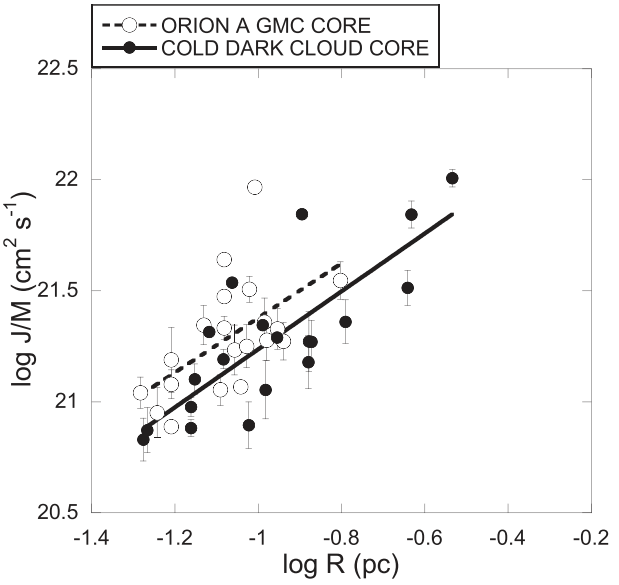

Fig. 7. Same as figure 5 but we use only cores with $R \geq 0.05$ pc and $v_{\rm rot} \geq 0.08$ km s^{-1}.

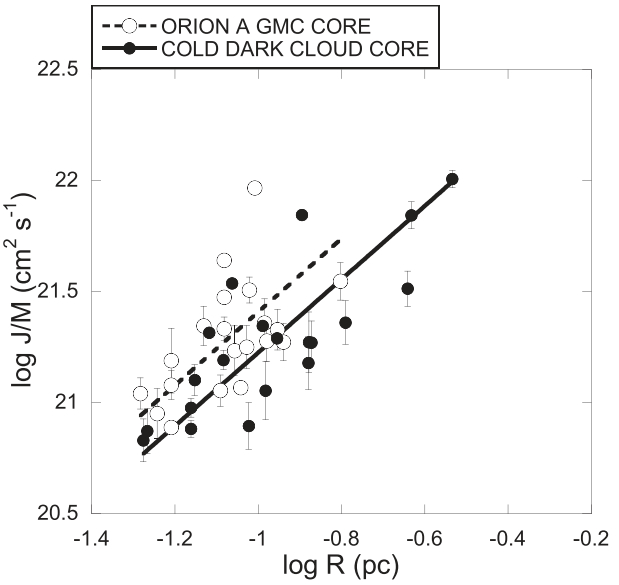

Fig. 8. Same as figure 7 but least-squares fitting is made by fixing the slope to 1.65.

to 1.65 for both the Orion and cold dark cloud cores above the Orion core detection limits (figure 8), we obtain

$$\log J/M\,(\mathrm{cm^2\ s^{-1}}) = 21.41 \pm 0.05 + 1.65 \log(R/0.1\ \mathrm{pc}) \quad (6)$$

for Orion cores,

$$\log J/M\,(\mathrm{cm^2\ s^{-1}}) = 21.23 \pm 0.05 + 1.65 \log(R/0.1\ \mathrm{pc}) \quad (7)$$

for cold dark cloud cores.

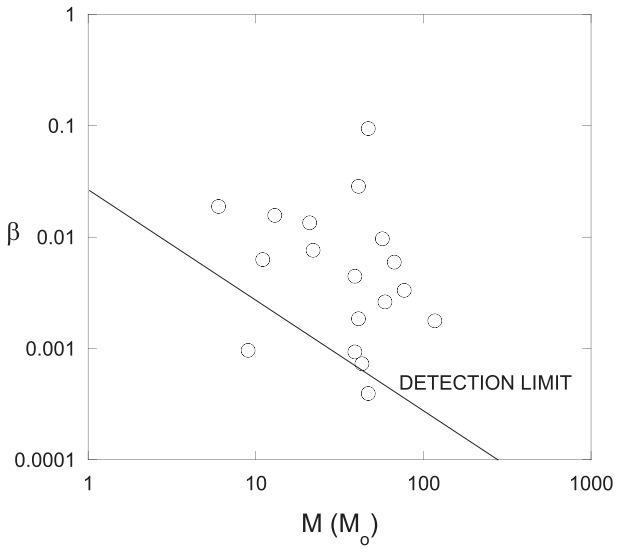

Fig. 9. Ratio β of rotational to gravitational energies is plotted against the core mass M. The thin straight line represent the approximate detection limit calculated by using $R = 0.05$ pc and $v_{\rm rot} = 0.08\,{\rm km\,s^{-1}}$.

3.2 Ratio of rotational to gravitational energies

The ratio β of rotational to gravitational energies is defined as $\beta = \frac{(1/2)I\omega^2}{qGM^2/R} = \frac{1}{2}\frac{p}{q}\frac{\omega^2 R^3}{GM}$ (for a uniform density sphere, $q = \frac{3}{5}$ and $p = \frac{2}{5}$; Goodman et al. 1993). We derived the logarithm of β to be -2.3 ± 0.7 for Orion N_2H^+ cores (without the restriction above). This is smaller than the value of the logarithm of β of -1.9 ± 0.7 for cold dark cloud cores. Note that β for cold dark cloud cores differs from that in Goodman et al. (1993) due to different definitions of R. If we take the virial mass $M_{\rm vir}$ instead of the core mass, we obtain the logarithm of β to be -2.0 ± 0.6 for Orion N_2H^+ cores. Taking into account a factor of two uncertainty in the absolute estimate of the core mass, we conclude that β is similar between Orion and cold dark cloud cores. We wonder how β depends on the core mass for Orion cores. Figure 9 plots β against the core mass M. It seems that β decreases with increasing core mass. This may mean that rotation is more important in low-mass cores. However, it is likely that this result is affected by the detection limit, because β is proportional to M^{-1} and also because cores have core radii and specific angular momenta close to the detection limits. The thin line in figure 9 represents the detection limit by using $R = 0.05$ pc and $v_{\rm rot} = 0.08\,{\rm km\,s^{-1}}$.

3.3 Properties of GMC cores

GMCs are likely to have deeper gravitational potentials due to their larger masses compared with cold dark clouds (e.g., Turner 1988). GMCs have larger pressure than cold dark clouds (e.g., Myers 1978; Turner 1988). This may mean that GMCs have higher ratios of molecular to atomic gas (Blitz & Rosolowsky 2006). Higher external pressure for cores will lead to larger non-thermal motions (turbulence or MHD wave) in cores (Chièze 1987). It seems that molecular clouds are only slightly supercritical, in various cloud scales from clouds to cores (Crutcher 2012), and GMC cores will tend to have stronger magnetic fields. Therefore, GMC cores will have larger intercepts in the power-law relation of the linewidth–size relation (Tatematsu et al. 1993). If we assume that turbulence or magnetic fields play an important role in the origin of the specific angular momentum, this might explain why GMC cores tend to have larger specific angular momentum J/M.

Another possibility is that the large overall specific angular momentum in the Orion A GMC (Imara & Blitz 2011), compared with other GMCs, results in a higher J/M. If the global specific angular momentum is related to the local specific angular momentum at the scale of molecular cloud cores, cores in the Orion A GMC might have larger specific angular momentum than those in other GMCs. It is suggested the Orion A GMC has a large angular momentum because it accompanies the richest OB associations (Blitz 1990). The same mechanism may work for Orion cores.

3.4 Comparison with global structure, global velocity gradient, core elongation, and molecular outflow

Kutner et al. (1977) measured the velocity gradient along the overall Orion A GMC for the first time, deriving a value of $0.135\,{\rm km\,s^{-1}\,pc^{-1}}$. The velocity gradient was observed along the elongation of the filamentary GMC, and they pointed out that the implied rotation is in the direction opposite to the Galactic rotation. Blitz (1990) found that the typical angular momentum of Galactic GMCs is less than half that of the Orion A GMC. The origin of the GMC velocity gradient is discussed in detail by Blitz (1993), Imara and Blitz (2011), and Imara, Bigiel, and Blitz (2011), including possibilities of the gradient inherited from the galaxy, that inherited from the parent interstellar medium (H I clouds), the sweeping action of the stellar association, the influence of magnetic fields including magnetic breaking (e.g., Field 1978), and so on. Tatematsu et al. (1993) found that the $\int$-shaped filament of the Orion A GMC shows a velocity gradient not only along the filament but also across the filament. The latter observed in the ^{13}CO $J = 1$–0 emission is ~ 2–$4\,{\rm km\,s^{-1}\,pc^{-1}}$, which is 20–40 times larger than the gradient along the filament. We wonder about the velocity gradients inside molecular cloud cores.

We investigate how the velocity gradient of cores is distributed in the Orion A GMC. Figure 10 shows the orientation of the velocity gradient on the N_2H^+ map. In

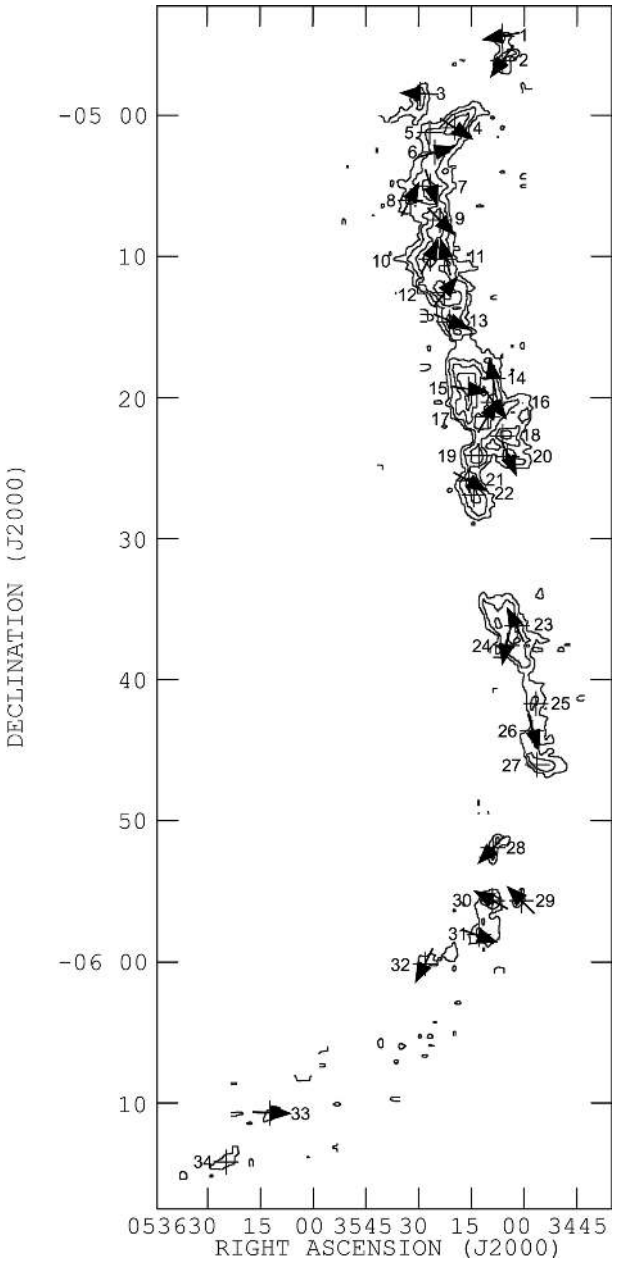

Fig. 10. Orientation of the velocity gradient is plotted for the N_2H^+ taken from Tatematsu et al. (2008). The contour map represents the velocity-integrated intensity of the N_2H^+ $J = 1$–0 $F_1 = 2$–1 hyperfine group. The contour levels are 0.749 K km s^{-1} × (1, 2, 4, 8). The intensity maxima of the N_2H^+ cores and the orientations of the velocity gradient are shown as pluses associated with core numbers and arrows, respectively.

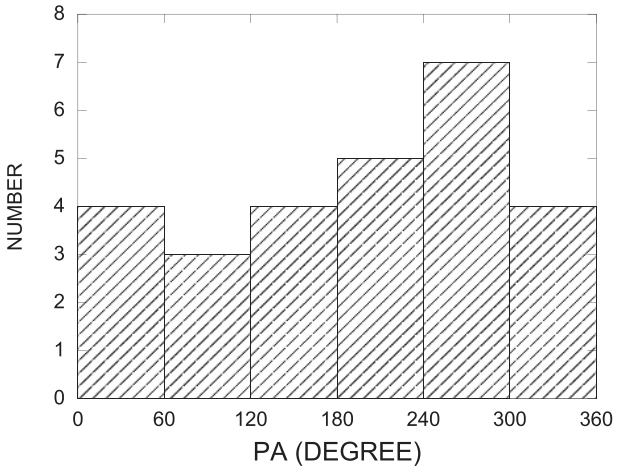

Fig. 11. Histogram of the orientation (position angle) of the velocity gradient for the Orion cores.

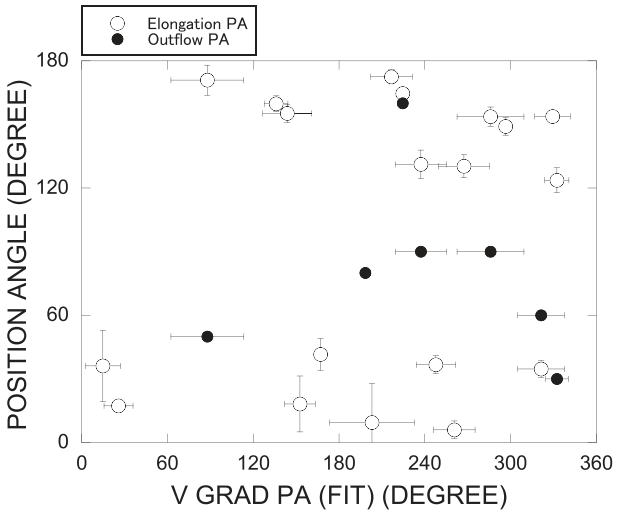

Fig. 12. Orientations of the elongation and the outflow lobe are plotted against the orientation of the velocity gradient.

figure 11, we plot the histogram of the position angle of the velocity gradient. We define $PA = 0^\circ$ if the core has a velocity gradient from south (negative velocity) to north (positive velocity). The gradient across the filament is a twisting motion with respect to Orion KL (Tatematsu et al. 1993). In the north of Orion KL, the eastern side of the filament has a more redshifted velocity, while in the south of Orion KL, the eastern side of the filament has a more blueshifted velocity (see their figure 3). In our *PA* definition, the *PA* of the velocity gradient is about 90° in the north of Orion KL and about 270° in the south of Orion KL. N_2H^+ cores 1–18 are located in the north of Orion KL and N_2H^+ cores 18–34 are located in the south of Orion KL (Tatematsu et al. 2008). There is no clear relation between the filament rotation across the filament and the core velocity gradients. We conclude that the filament rotation across the filament does not likely govern the core rotation. The global velocity gradient direction along the GMC elongation for the Orion A GMC, which is much smaller than the gradient across the filament, corresponds to $PA \sim 330^\circ$ in our definition. The velocity gradients of cores are not significantly related to the global gradient. It seems that the origin of the specific angular momentum is not a simple top-down collapse from larger structures—cf. Imara and Blitz (2011) for H I cloud–GMC comparison.

Table 3. Position angle of the core elongation and the associated molecular outflow for Orion A GMC N_2H^+ cores.

No.	Elongation *PA* (°)	Angle between V Grad and elongation (°)	Outflow	Outflow *PA* (°)
1	–	–	–	–
2	155.2 ± 4.3	11.4	–	–
3	170.9 ± 7.1	83.0	OMC-3 SIMBA a, SIMBA c	50
4	131.2 ± 6.7	73.9	OMC-3 MMS2	90
5	–	–	–	–
6	153.7 ± 4.5	47.7	OMC-3 MMS7	90
7	–	–	OMC-3 MMS9	80
8	123.7 ± 5.9	28.7	–	–
9	164.6 ± 0.8	60.0	OMC-2 FIR1b	160
10	–	–	OMC-2 FIR3	30
11	36.1 ± 16.9	21.2	–	–
12	34.7 ± 4.0	73.3	OMC-2 FIR6b	60
13	36.7 ± 4.2	31.1	–	–
14	–	–	–	–
15	6.0 ± 4.2	74.7	–	–
16	172.5 ± 3.4	44.2	–	–
17	153.8 ± 0.6	4.4	–	–
18	–	–	–	–
19	–	–	Orion-S	35
20	9.4 ± 18.4	13.7	–	–
21	–	–	–	–
22	–	–	–	–
23	17.3 ± 1.8	8.5	–	–
24	41.6 ± 7.5	54.5	–	–
25	–	–	–	–
26	149.1 ± 4.1	32.5	–	–
27	–	–	–	–
28	159.8 ± 3.7	23.8	–	–
29	–	–	–	–
30	–	–	–	–
31	–	–	–	–
32	18.2 ± 13.2	45.5	–	–
33	130.3 ± 5.4	42.9	–	–
34	–	–	–	–

We wonder whether the velocity gradient is related to the core elongation. If rotation is dominant in core support, these will be positively correlated. We plot the orientation of the elongation against the orientation of the velocity gradient in figure 12. The *PA* of the core elongation is measured by using the half-intensity contour on the four position–velocity diagrams passing through the core center, and fit the sinusoidal curve on the core size–*PA* diagram (table 3). We failed to measure the core elongation in eight cores (out of 27), because they are almost circular or far from elliptical (irregular). In these cases, elongation is blank in the table. Core elongation has a deficit for $PA = 60^\circ$ to 120°. Figure 13 shows the histogram of the *PA* of the core elongation. This means that cores having an elongation perpendicular to the global filament are rare. In figure 14,

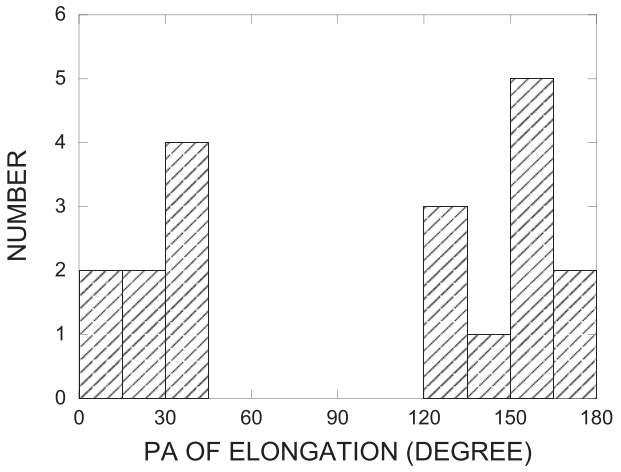

Fig. 13. Histogram of the core elongation for the Orion cores.

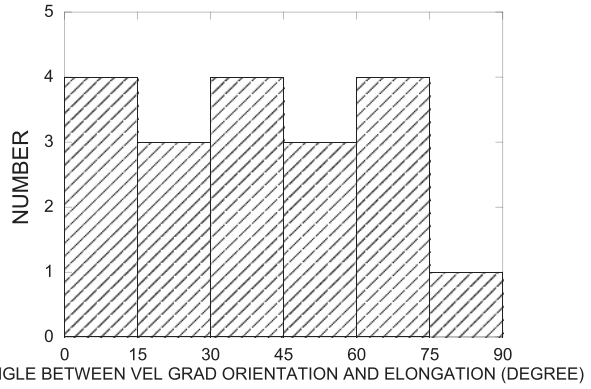

Fig. 14. Histogram of the angle between the orientation of the velocity gradient and core elongation for the Orion cores.

we plot the histogram of the angle between the velocity gradients and elongations of the cores. There is a decrease of cores with the velocity gradient perpendicular to the core elongation. However, this could be due to selection effects, since it is harder to measure the gradient across the elongation due to limited resolution. Except for this depression, there is no clear tendency between the velocity gradient and the core elongation. Rotationally supported oblate cores will show velocity gradients parallel to the core elongation, but we do not see such a peak. This is naturally understood, because β is small.

Next, we discuss the relationship between the orientations of the velocity gradient, the molecular outflow, and the magnetic fields. Matsumoto and Tomisaka (2004) have studied the relationship between the magnetic field direction and the resulting orientation of outflows/jets theoretically. They concluded that outflows tend to be aligned with magnetic fields of the parent cloud. Molecular outflows in the OMC-2/3 region were studied by Aso et al. (2000), Yu et al. (2000), Shimajiri et al. (2008), and Takahashi et al. (2008). In addition, we include a molecular outflow associated with Orion-S observed by Schmidt-Burgk et al. (1990). We list molecular outflows, with driving source names from Chini et al. (1997) and Nielbock, Chini, and Muller (2003), and their lobe orientation from Takahashi et al. (2008) in table 3, and they are also plotted in figure 12. The "Outflow" column in table 3 lists only outflows with measurable lobe directions. We wonder if magnetic field orientation is related to any of the above orientations. Poidevin, Bastien, and Matthews (2010) have shown the distribution of the magnetic field orientation for the OMC-2/3 region. They concluded that no correlation is evident between the relative orientation of jets or outflows and the magnetic field. The *PA* of the magnetic field is $\sim 135^\circ$ near MMS2 and MMS7, while it is $\sim 90^\circ$ near MMS9. Due to the limited number of outflows having well-defined orientations, it is hard to reach any clear conclusion, but at least we can say that we do not see any very strong correlation among these orientations in tables 2 and 3.

3.5 Dependence on the molecular line employed

Lastly, we discuss how our result could depend on the selected molecular lines. If we analyze the velocity gradient on the basis of observations with different molecular lines, the results could be different (e.g., Goodman et al. 1993). We used N_2H^+ observations for Orion cores, while Goodman et al. (1993) used NH_3 for cold dark cloud cores. In general, N_2H^+ and NH_3 show rather similar distributions, compared with other molecules such as CCS, CS, $C^{18}O$, and $C^{17}O$ (e.g., Tafalla et al. 2002; Aikawa et al. 2001 for L1544 and other starless cold dark cloud cores). Therefore, we expect N_2H^+ and NH_3 to trace similar volumes. On the other hand, Hotzel, Harju, and Walmsley (2004) reported changes in the abundance ratio of NH_3 to N_2H^+. In the future, it is desirable to check our result by using the same molecular line, the same core identification, and velocity gradient measurement method with comparable linear spatial resolutions in pc.

4 Summary

We have analyzed the specific angular momentum of molecular cloud cores in the Orion A giant molecular cloud using the N_2H^+ data of Tatematsu et al. (2008). We have measured the velocity gradient using four position–velocity diagrams passing through the core centers with $PA = 0^\circ$, 45°, 90°, and 135°, and made a sinusoidal fitting on the velocity gradient–*PA* diagram. By comparing with the J/M–R relation, we marginally found that the Orion N_2H^+ cores have systematically larger J/M than the cold dark cloud cores of Goodman et al. (1993). The logarithm of the ratio of rotational to gravitational energies is $\log \beta = -2.3 \pm 0.7$ and -1.9 ± 0.7 for Orion N_2H^+ cores and cold dark cloud cores, respectively. The large-scale rotation of the $\int$-shaped filament of the Orion A GMC does not likely govern the core rotation at smaller scales. During the analysis, we also found that cores elongated perpendicular to the large-scale filament are rare.

Acknowledgement

We wish to thank an anonymous referee for very valuable constructive comments that have significantly improved the presentation of the paper.

References

Aikawa, Y., Ohashi, N., Inutsuka, S., Herbst, E., & Takakuwa, S. 2001, ApJ, 552, 639

Aso, Y., Tatematsu, K., Sekimoto, Y., Nakano, T., Umemoto, T., Koyama, K., & Yamamoto, S. 2000, ApJS, 131, 465
Ballesteros-Paredes, J., Hartmann, L. W., Vázquez-Semadeni, E., Heitsch, F., & Zamora-Avilés, M. A. 2011, MNRAS, 411, 65
Bergin, E. A., Alves, J., Huard, T. L., & Tafalla, M. 2002, ApJ, 570, L101
Bergin, E. A., Ciardi, D. R., Lada, C. J., Alves, J., & Lada, E. A. 2001, ApJ, 557, 209
Bergin, E. A., & Tafalla, M. 2007, ARA&A, 45, 339
Blitz, L. 1990, ASP Conf. Ser., 12, 273
Blitz, L. 1993, in Protostars and Planets III, ed. E. H. Levy & J. I. Lunine (Tucson: University of Arizona Press), 125
Blitz, L., & Rosolowsky, E. 2006, ApJ, 650, 933
Bodenheimer, P. 1995, ARA&A, 33, 199
Caselli, P., & Myers, P. C. 1995, ApJ, 446, 665
Caselli, P., Myers, P. C., & Thaddeus, P. 1995, ApJ, 455, L77
Chièze, J. P. 1987, A&A, 171, 225
Chini, R., Reipurth, B., Ward-Thompson, D., Bally, J., Nyman, L.-Å., Sievers, A., & Billawala, Y. 1997, ApJ, 474, L135
Crutcher, R. M. 2012, ARA&A, 50, 29
Danby, G., Flower, D. R., Valiron, P., Schilke, P., & Walmsley, C. M. 1988, MNRAS, 235, 229
Field, G. B. 1978, in Protostars and Planets, ed. T. Gehrels (Tucson: University of Arizona Press), 243
Fuller, G. A., & Myers, P. C. 1992, ApJ, 384, 523
Genzel, R., & Stutzki, R. 1989, ARA&A, 27, 41
Goldsmith, P. F., & Arquilla, R. A. 1985, in Protostars and Planets II, ed. D. C. Black & M. S. Mathews (Tucson: Univesity of Arizona Press), 137
Goodman, A. A., Benson, P. J., Fuller, G. A., & Myers, P. C. 1993, ApJ, 406, 528
Heyer, M. H, Krawczyk, C., Duval, J., & Jackson, J. M. 2009, ApJ, 699, 1092
Hotzel, S., Harju, J., & Walmsley, C. M. 2004, A&A, 415, 1065
Ikeda, N., Sunada, K., & Kitamura, Y. 2007, ApJ, 665, 1194
Imara, N., Bigiel, F., & Blitz, L. 2011, ApJ, 732, 79
Imara, N., & Blitz, L. 2011, ApJ, 732, 78
Inoue, T., & Inutsuka, S. 2012, ApJ, 759, 35
Kim, M. K., et al. 2008, PASJ, 60, 991
Kutner, M. L., Tucker, K. D., Chin, G., & Thadeus, P. 1977, ApJ, 215, 521
Larson, R. B. 1981, MNRAS, 194, 809
Lee, J-.E., Bergin, E. A., & Evans, N. J., II 2004, ApJ, 617, 360
MacLaren, I, Richardson, K. M., & Wolfendale, A. W. 1988, ApJ, 333, 821
Matsumoto, T., & Hanawa, T. 2003, ApJ, 595, 913
Matsumoto, T., & Tomisaka, K. 2004, ApJ, 616, 266
Miyama, S. M., Hayashi, C., & Narita, S. 1984, ApJ, 279, 621
Myers, P. C. 1978, ApJ, 225, 380
Myers, P. C. 1983, ApJ, 270, 105
Nielbock, M., Chini, R., & Muller, S. A. H. 2003, A&A, 408, 245
Onishi, T., Mizuno, A., Kawamura, A., Tachihara, K., & Fukui, Y. 2002, ApJ, 575, 950
Poidevin, F., Bastien, P., & Matthews, B. C. 2010, ApJ, 716, 893
Schmid-Burgk, J., Güsten, R., Mauersberger, R., Schulz, A., & Wilson, T. L. 1990, ApJ, 362, L25
Shimajiri, Y., Takahashi, S., Takakuwa, S., Saito, M., & Kawabe, R. 2008, ApJ, 638, 255
Shu, F. H., Adams, F. C., & Lizano, S. 1987, ARA&A, 25, 23
Tafalla, M., Myers, P. C., Caselli, P., Walmsley, C. M., & Comito, C. 2002 ApJ, 569, 815
Takahashi, S., Saito, M., Ohashi, N., Kusakabe, N., Takakuwa, S., Shimajiri, Y., Tamura, M., & Kawabe, R. 2008, ApJ, 688, 344
Tatematsu, K., et al. 1993, ApJ, 404, 643
Tatematsu, K. 1999, in Star Formation 1999, ed. T. Nakamoto (Nobeyama: Nobeyama Radio Observatory), 72
Tatematsu, K., et al. 2014, PASJ, 66, 16
Tatematsu, K., Kandori, R., Umemoto, T., & Sekimoto, Y. 2008, PASJ, 60, 407
Traficante, A., Fuller, G. A., Smith, R., Billot, N., Duarte-Cabral, A., Peretto, N., Molinari, S., & Pineda, J. E. 2015, MNRAS submitted (arXiv:1511.03670)
Tsuboi, M., & Miyazaki, A. 2012, PASJ, 64, 111
Tsuribe, T., & Inutsuka, S. 1999, ApJ, 523, L155
Turner, B. E. 1988, in Galactic and Extragalactic Radio Astronomy, 2nd ed., ed. G. L. Vershuur & K. I. Kellermann (New York: Springer-Verlag), 154
Wilson, T. L., Mauersberger, R., Gensheimer, P. D., Muders, D., & Bieging, J. H. 1999, ApJ, 525, 343
Womack, M., Ziurys, L. M., & Sage, L. J. 1993, ApJ, 406, L29
Yu, K. C., Billawala, Y., Smith, M. D., Bally, J., & Butner, H. M. 2000, ApJ, 120, 1974